Nonlinear Analysis: Real World Applications 12 (2011) 1681–1697

Contents lists available at ScienceDirect

Nonlinear Analysis: Real World Applications

journal homepage: www.elsevier.com/locate/nonrwa

Closure method for spatially averaged dynamics of particle chains

Alexander Panchenko [a], Lyudmyla L. Barannyk [b], Robert P. Gilbert [c,*]

[a] Department of Mathematics, Washington State University, Pullman, WA 99164, United States
[b] Department of Mathematics, University of Idaho, Moscow, ID 83843, United States
[c] Department of Mathematical Sciences, University of Delaware, Newark, DE 19716, United States

ARTICLE INFO

Article history:
Received 25 October 2010
Accepted 29 October 2010

Keywords:
FPU chain
Particle chain
Oscillator chain
Upscaling
Model reduction
Dimension reduction
Closure problem

ABSTRACT

We study the closure problem for continuum balance equations that model the mesoscale dynamics of large ODE systems. The underlying microscale model consists of classical Newton equations of particle dynamics. As a mesoscale model we use the balance equations for spatial averages obtained earlier by a number of authors: Murdoch and Bedeaux, Hardy, Noll and others. The momentum balance equation contains a flux (stress), which is given by an exact function of particle positions and velocities. We propose a method for approximating this function by a sequence of operators applied to the average density and momentum. The resulting approximate mesoscopic models are systems in closed form. The closed form property allows one to work directly with the mesoscale equations without the need to calculate the underlying particle trajectories, which is useful for the modeling and simulation of large particle systems. The proposed closure method utilizes the theory of ill-posed problems, in particular iterative regularization methods for solving first order linear integral equations. The closed form approximations are obtained in two steps. First, we use Landweber regularization to (approximately) reconstruct the interpolants of the relevant microscale quantities from the average density and momentum. Second, these reconstructions are substituted into the exact formulas for stress. The developed general theory is then applied to non-linear oscillator chains. We conduct a detailed study of the simplest zero-order approximation, and show numerically that it works well as long as the fluctuations of velocity are nearly constant.

1. Introduction

In a series of papers, [1–4], Murdoch and Bedeaux studied continuum mechanical balance equations for the mesoscopic space time averages of discrete systems. The earlier work of Irving and Kirkwood [5], Noll [6], and Hardy [7] on closely related topics should be also mentioned here. The fluxes in balance equations (e.g. stress) are given by exact formulas as functions of particle positions and velocities. This is useful for linking microscale dynamics with mesoscale phenomena. However, using these formulas requires a complete knowledge of underlying particle dynamics. Since many particle systems of interest have an enormous size, the direct simulation of particle trajectories may be intractable. Consequently, it makes sense to look for closed form approximations of fluxes in terms of other mesoscale quantities (e.g., average density and velocity), rather than microscopic variables.

In this paper we address the above closure problem for the spatially averaged mesoscale dynamics of large size classical particle chains. The design of the method was influenced by the following considerations.

* Corresponding author.
E-mail addresses: panchenko@math.wsu.edu (A. Panchenko), barannyk@uidaho.edu (L.L. Barannyk), gilbert@math.edul.edu, gilbert@math.udel.edu (R.P. Gilbert).

1468-1218/$ – see front matter © 2011 Published by Elsevier Ltd
doi:10.1016/j.nonrwa.2010.10.021

(1) The quantities of interest are space–time continuum averages, such as density, linear momentum, stress, energy and others. This choice of averages is natural because these quantities are experimentally measurable, and also because of their importance in coupled multiscale simulations involving both continuum and discrete models. In addition, by working directly with space–time averages instead of ensemble averages one can bypass a difficult problem of relating probabilistic and space–time averages.

(2) It is desirable to be able to predict the behavior of averages on arbitrary time intervals, no matter how short. This perspective comes from PDE problems, where the observation time is often arbitrary and the long time behavior is not of interest. When one tracks ODE systems on an arbitrary time interval, transients may be all that are observed. Therefore, we do not use the qualitative theory of ODEs, primarily concerned with describing the long time features of dynamics. This significantly decreases the range of available tools. However, the closure problem for mesoscopic PDEs turned out to be a question that can be still answered in a satisfactory way. The methods developed in this fashion can be helpful in situations where long time features are not of interest: modeling transient and short-lived phenomena, working with metastable systems, and dealing with problems for which the relaxation times can be hard to estimate.

(3) We consider particle systems with initial conditions that either are known precisely, or are at least such that the possible initial positions and velocities are strongly restricted by available a priori information. This is in contrast to statistical mechanics, where uncertainty of the initial conditions is a major problem. In this regard we note that our approach makes sense for discrete models of solid–fluid continuum systems, where the smallest relevant length scale is still much larger than a typical intermolecular distance. For other particle systems, our method can be used to run deterministic simulations repeatedly, in order to accumulate statistical information about the underlying probability density.

(4) Because of the widespread use of computers in physical and engineering sciences, it is useful to develop theories tailored for computation, rather than "paper and pencil" modeling. As far as the closure problem is concerned, the traditional phenomenological approach to formulating constitutive equations can be subsumed by a more general problem of finding a computational closure method. In particular, a closure method can be realized as an iterative procedure where one inputs the values of the primary variables (e.g. density and velocity) computed at the previous moment of time, and the algorithm generates the flux (e.g. stress) at the next moment. Then primary variables are updated using mesoscopic balance equations, and the process is repeated. In addition, focusing on computing one can obtain unconventional but useful continuum mechanical models. By replacing a simple, but possibly crude, Taylor series truncation with an algorithm we make it harder to obtain exact solutions. Since such solutions are rarely available even for simple classical systems, (e.g. Navier–Stokes equations), this is not a serious drawback. On the positive side, computational closure generally contains an explicit (explicitly computable) link between micro- and mesoscale properties.

(5) An important potential application of closure is the development of fast numerical methods for simulating the mesoscopic dynamics of particle systems. Mesoscale solvers usually employ coarse meshes with a mesh size much larger than a typical interparticle distance. Then the averages would usually be given by their coarse mesh values, while interpolants of microscale quantities are discretized on a fine scale mesh. Consequently, a closure method might consist of two generic blocks: (i) reconstruction on a mesoscale mesh whereby coarse approximations of fine scale quantities are obtained from averages; and (ii) interpolation of the obtained coarse scale discretizations to fine scale.

The closure algorithm developed in this paper is based on iterative regularization methods for solving first kind integral equations. We observe that primary mesoscale averages are related to the interpolants of microscale variables via a linear convolution operator. The kernel of this operator is the "window function" used in [1] to generate averages. Such integral operators are usually compact. A compact operator may be invertible, but the inverse operator is not continuous. Therefore, the problem of reconstructing microscale quantities from given averages is ill-posed. Such problems are well studied in the literature [8–12]. A particular method used in this paper for inverting convolutions is the Landweber iteration [13,14]. It is known that if the error in the data tends to zero, the Landweber method produces successive approximations converging to the exact solution. For the merely bounded data error, convergence is replaced by a stopping criterion. This criterion provides the optimal number of iterations needed to approximate the solution with the accuracy proportional to the error in the data. As a consequence, our method has a desirable feature: one can improve the approximation quality at the price of increasing the algorithm complexity. This means that predictive capability of the method can be regulated depending on the available computing power.

This paper is organized as follows. In Section 2 we describe a general multi-dimensional microscopic model. The equations of motion are classical Newton equations. We limit ourselves to the case of short range interaction forces that may be either conservative or dissipative. The scaling of particle masses and forces reflects a continuum mechanical perspective; that is a family of particle systems of increasing size should represent a hypothetical continuum material. As $N \to \infty$, the total mass of the system should remain fixed, and the total particle energy should be either fixed, or at least bounded independent of N. Next, we recall the main points of averaging theory of Murdoch–Bedeaux and provide mesoscopic balance equations and exact formulas for the stress from [4]. In Section 3 we develop integral approximations of averages, and describe the use of Landweber iterative regularization for approximate reconstruction. Section 4 contains the formulation of the scaled ODE equations of the so-called Fermi–Pasta–Ulam (FPU) chains. In Section 5 we derive closed form mesoscopic

continuum equations of chain dynamics. The complexity of these continuum models increases with the order n of the iterative deconvolution approximation. Section 6 is devoted to the detailed study of the simplest closed model with $n = 0$, which we call zero-order closure. Essentially, zero-order closure means that the microscopic quantities are replaced by their averages. Such an approximation can only work well for systems with small fluctuations. To quantify the fluctuation size we introduce upscaling temperature and the related notion of quasi-isothermal dynamics. For such dynamics, we show how to interpolate averages given by mesoscopic mesh values, in order to initialize approximate particle positions and velocities. The interpolation procedure is problem-specific: it conserves the microscopic energy and preserves the quasi-isothermal nature of the dynamics. Section 7 contains the results of computational tests. Here we apply our zero-closure algorithm to a Hamiltonian chain with the finite range repulsive potential U, decreasing as a power of distance. The results show good agreement of zero-order approximations with the exact stress produced by direct simulations with 10,000–80,000 particles, provided the initial conditions have small fluctuations. In our example, the initial conditions are such that the upscaling temperature is nearly zero during the observation time. We also demonstrate that increasing fluctuation of the initial velocities leads to a considerable increase in the approximation error, indicating that higher order closure algorithms should be used instead of zero-order closure. The applicability of the zero-order closure is further discussed in Section 8. Finally, conclusions are provided in Section 9.

2. Microscale equations and mesoscale spatial averages

2.1. Scaled ODE problems

The starting point is the microscale ODE problem. In this paper we shall work with classical Newton equations of point particle dynamics. The same equations may arise as discretization of the momentum balance equation for continuum systems. Consider a system containing $N \gg 1$ identical particles, denoted by P_i. The mass of each particle is $\frac{M}{N}$, where M is the total mass of the system. Suppose that during the observation time T, P_i remain inside a bounded domain Ω in $\mathbb{R}^d$, where d is the physical space dimension, usually 1, 2 or 3. The positions $\boldsymbol{q}_i(t)$ and velocities $\boldsymbol{v}_i(t)$ of particles satisfy a system of ODEs

$$\dot{\boldsymbol{q}}_i = \boldsymbol{v}_i, \tag{2.1}$$

$$\frac{M}{N}\dot{\boldsymbol{v}}_i = \boldsymbol{f}_i + \boldsymbol{f}_i^{(\mathrm{ext})}, \tag{2.2}$$

subject to the initial conditions

$$\boldsymbol{q}_i(0) = \boldsymbol{x}_i, \qquad \boldsymbol{v}_i(0) = \boldsymbol{v}_i^0. \tag{2.3}$$

Here $\boldsymbol{f}_i^{(\mathrm{ext})}$ denotes external forces, such as gravity and confining forces. The interparticle forces $\boldsymbol{f}_i = \sum_j \boldsymbol{f}_{ij}$, where $\boldsymbol{f}_{ij}$ are pair interaction forces which depend on the relative positions and velocities of the respective particles.

We are interested in investigating asymptotic behavior of the system as $N \to \infty$. Thus it is convenient to introduce a small parameter

$$\varepsilon = N^{-1/d}, \tag{2.4}$$

characterizing a typical distance between neighboring particles. As ε approaches zero, the number of particles goes to infinity, and the distances between neighbors shrinks. Consequently, the forces in (2.2) should be properly scaled. The guiding principle for scaling is to make the energy of the system bounded independent of N, as $N \to \infty$. In addition, the energy of the initial conditions should be bounded uniformly in N.

As an example of scaling, consider the forces generated by a finite range potential U and assume that each particle interacts with no more than a fixed number of neighbors (this is the case, e.g., for particle chains with nearest neighbor interaction, where a particle always interacts with two neighbors). The fixed number of interacting neighbors implies that there are about N interacting pairs. Assuming also that the system is sufficiently dense, and the variations of particle concentrations are not large, we can suppose that a typical distance between interacting particles is on the order $N^{-1/d}L = \varepsilon L$. The resulting scaling

$$\boldsymbol{f}_{ij} = -\frac{1}{\varepsilon N}\nabla_{\boldsymbol{x}} U\left(\frac{\boldsymbol{q}_i - \boldsymbol{q}_j}{\varepsilon}\right) \tag{2.5}$$

makes the potential energy of an isolated system bounded independent of N. The kinetic energy will be under control provided the total energy of the initial conditions is bounded independent of N. If exterior forces are present, they should be scaled as well.

Remark. Superficially, the system (2.1), (2.2) looks similar to the parameter-dependent ODE systems studied in numerous works on ODE time homogenization (see e g. [15] and references therein). In the problem under study, ε depends on the *system dimension* N, while in the works on time-homogenization and ODE perturbation theory, the system size is usually fixed as $\varepsilon \to 0$.

2.2. Length scales

We introduce the following length scales:

- macroscopic length scale $L = \mathrm{diam}(\Omega)$;
- microscopic length scale εL;
- mesoscopic length scale ηL,

where $0 < \eta < 1$ is a parameter that characterizes the spatial mesoscale resolution. This parameter is chosen based on the desired accuracy, the computational cost requirements, the available information about initial conditions and behavior of ODE trajectories etc.

The computational domain Ω is subdivided into mesoscopic cells C_β, $\beta = 1, 2, \ldots, B$, with the side length on the order of ηL. The centers $\boldsymbol{x}_\beta$ of C_β are the nodes of the meso-mesh. The number of unknowns in the mesoscopic system will be on the order of B. For computational efficiency, one should have $B \ll N$. This does not mean that η is close to one. In fact, it makes sense to keep η as small as possible in order to have an additional asymptotic control over the system behavior. Decreasing η will in general make computations more expensive.

2.3. Averages and their evolution

To define averages we first select a fast decreasing window function ψ satisfying $\int \psi(\boldsymbol{x})\mathrm{d}\boldsymbol{x} = 1$. There are many possible choices of the window function. In this paper we assume, unless otherwise indicated, that ψ is a compactly supported, differentiable on the interior of its support, and non-negative. Next, define

$$\psi_\eta(\boldsymbol{x}) = \eta^{-d}\psi\left(\frac{\boldsymbol{x}}{\eta}\right).$$

Once the window function is chosen, we can evaluate the averages of various continuum mechanical variables, following [1,4]. The mesoscopic average density and momentum are given by

$$\overline{\rho}^\eta(t, \boldsymbol{x}) = \frac{M}{N}\sum_{i=1}^{N}\psi_\eta(\boldsymbol{x} - \boldsymbol{q}_i(t)), \tag{2.6}$$

$$\overline{\rho}^\eta\overline{\boldsymbol{v}}^\eta(t, \boldsymbol{x}) = \frac{M}{N}\sum_{i=1}^{N}\boldsymbol{v}_i(t)\psi_\eta(\boldsymbol{x} - \boldsymbol{q}_i(t)). \tag{2.7}$$

The meaning of the above definitions becomes clear if one considers $\psi = (c_d)^{-1}\chi(x)$, where χ is a characteristic function of the unit ball in $\mathbb{R}^d$, and c_d is the volume of the unit ball. Then

$$\overline{\rho}^\eta = \frac{1}{c_d\eta^d}\frac{M}{N}\sum_{i=1}^{N}\chi\left(\frac{\boldsymbol{x} - \boldsymbol{q}_i(t)}{\eta}\right).$$

The sum in the right hand side gives the number of particles located within distance η of $\boldsymbol{x}$ at time t. Multiplying by M/N we get the total mass of these particles, and dividing by $c_d\eta^d$ (the volume of η-ball) gives the usual particle density.

Differentiating (2.6), (2.7) in t, and using the ODEs (2.1), (2.2) one can obtain [1] exact mesoscopic balance equations for all primary variables. For example, for an isolated system with ($\boldsymbol{f}_i^{(\mathrm{ext})} = 0$), the mass conservation and momentum balance equations take the form:

$$\partial_t\overline{\rho}^\eta + \mathrm{div}(\rho^\eta\overline{\boldsymbol{v}}^\eta) = 0, \tag{2.8}$$

$$\partial_t(\overline{\rho}^\eta\overline{\boldsymbol{v}}^\eta) + \mathrm{div}(\overline{\rho}^\eta\overline{\boldsymbol{v}}^\eta \otimes \overline{\boldsymbol{v}}^\eta) - \mathrm{div}\boldsymbol{T}^\eta = 0. \tag{2.9}$$

The stress $\boldsymbol{T}^\eta = \boldsymbol{T}^\eta_{(c)} + \boldsymbol{T}^\eta_{(\mathrm{int})}$ [4], where

$$\boldsymbol{T}^\eta_{(c)}(t, \boldsymbol{x}) = -\sum_{i=1}^{N} m_i(\boldsymbol{v}_i - \overline{\boldsymbol{v}}^\eta(t, \boldsymbol{x},)) \otimes (\boldsymbol{v}_i - \overline{\boldsymbol{v}}^\eta(\boldsymbol{x}, t))\psi(\boldsymbol{x} - \boldsymbol{q}_i) \tag{2.10}$$

is the *convective stress*, and

$$\boldsymbol{T}^\eta(t, \boldsymbol{x})_{(\mathrm{int})} = \sum_{(i,j)}\boldsymbol{f}_{ij} \otimes (\boldsymbol{q}_j - \boldsymbol{q}_i)\int_0^1 \psi(s(\boldsymbol{x} - \boldsymbol{q}_j) + (1 - s)(\boldsymbol{x} - \boldsymbol{q}_i))\mathrm{d}s \tag{2.11}$$

is the *interaction stress*. The summation in (2.11) is over all pairs of particles (i, j) that interact with each other.

Discretizing balance equations on the mesoscopic mesh yields a discrete system of equations, called the *meso-system*, written for mesh values of $\overline{\rho}^\eta_\beta$, $(\overline{\rho}^\eta\overline{\boldsymbol{v}}^\eta)_\beta$ and $\boldsymbol{T}^\eta_\beta$. The dimension of the meso-system is much smaller than the dimension of the original ODE problem. However, at this stage we still have no computational savings, since the meso-system is *not closed*. This means that mesoscopic fluxes such as (2.10), (2.11) are expressed as functions of the microscopic positions and velocities. To find these positions and velocities, one has to solve the original microscale system (2.1), (2.2). To achieve

computational savings we need to replace exact fluxes with approximations that involve only mesoscale quantities. We refer to the procedure of generating such approximations as a **closure method**. This closure-based approach has much in common with continuum mechanics. The important difference is that the focus is on computing, rather than continuum mechanical style modeling of constitutive equations.

3. Closure via regularized deconvolutions

3.1. Outline

Our approach is based on a simple idea: the integral approximations of primary averages (such as density and velocity) are related to the corresponding microscopic quantities via convolution with the kernel ψ_η. Therefore, given primary variables we can (approximately) recover the microscopic positions and velocities by numerically inverting the convolution operators. The results are inserted into equations for secondary averages (or fluxes), such as stress in the momentum balance. This yields closed form balance equations that can be simulated efficiently on the mesoscopic mesh.

3.2. Integral approximation of discrete averages

To exploit the special structure of primary averages, it is convenient to approximate sums such as

$$\overline{g}^\eta = \frac{1}{N}\sum_{j=1}^{N} g(\boldsymbol{v}_j, \boldsymbol{q}_j)\psi_\eta(\boldsymbol{x} - \boldsymbol{q}_j) \tag{3.1}$$

by integrals. Since particle positions $\boldsymbol{q}_j$ are not periodically spaced, (3.1) is not in general a Riemann sum for $g\psi_\eta(\boldsymbol{x} - \cdot)$. To interpret the sum correctly, we introduce interpolants $\tilde{\boldsymbol{q}}(t, \boldsymbol{X})$, $\tilde{\boldsymbol{v}}(t, \tilde{\boldsymbol{q}})$ of positions and velocities, associated with the microscopic ODE system (2.1), (2.2). At $t = 0$ these interpolants satisfy

$$\tilde{\boldsymbol{q}}(0, \boldsymbol{X}_j) = \boldsymbol{q}_j^0, \qquad \tilde{\boldsymbol{v}}(0, \tilde{\boldsymbol{q}}(0, \boldsymbol{X}_j)) = \boldsymbol{v}_j^0,$$

where $\boldsymbol{X}_j, j = 1, 2, \ldots, N$ are points of ε-periodic rectangular lattice in Ω. At other times,

$$\tilde{\boldsymbol{q}}(t, \boldsymbol{X}_j) = \boldsymbol{q}_j(t), \qquad \tilde{\boldsymbol{v}}(t, \tilde{\boldsymbol{q}}(t, \boldsymbol{X}_j)) = \boldsymbol{v}_j(t).$$

Then we can rewrite (3.1) as

$$\overline{g}^\eta = \frac{1}{|\Omega|}\sum_{j=1}^{N} \frac{|\Omega|}{N} g(\tilde{\boldsymbol{v}}(t, \tilde{\boldsymbol{q}}(t, \boldsymbol{X}_j)), \tilde{\boldsymbol{q}}(t, \boldsymbol{X}_j))\psi_\eta(\boldsymbol{x} - \tilde{\boldsymbol{q}}(t, \boldsymbol{X}_j)), \tag{3.2}$$

where $|\Omega|$ denotes the volume (Lebesgue measure) of Ω. Eq. (3.2) is a Riemann sum generated by partitioning Ω into N cells of volume $|\Omega|/N$ centered at $\boldsymbol{X}_j$. This yields

$$\overline{g}^\eta = \frac{1}{|\Omega|}\int_\Omega g(\tilde{\boldsymbol{v}}(t, \tilde{\boldsymbol{q}}(t, \boldsymbol{X})), \tilde{\boldsymbol{q}}(t, \boldsymbol{X}))\psi_\eta(\boldsymbol{x} - \tilde{\boldsymbol{q}}(t, \boldsymbol{X}))\mathrm{d}\boldsymbol{X}, \tag{3.3}$$

up to discretization error. Now suppose that the map $\tilde{\boldsymbol{q}}(\cdot, \boldsymbol{X})$ is invertible for each t, that is $\boldsymbol{X} = \tilde{\boldsymbol{q}}^{-1}(t, \tilde{\boldsymbol{q}})$. Changing the variables in the integral $\boldsymbol{y} = \tilde{\boldsymbol{q}}(t, \boldsymbol{X})$ we obtain a generic integral approximation

$$\overline{g}^\eta = \frac{1}{|\Omega|}\int_\Omega g(\tilde{\boldsymbol{v}}(t, \boldsymbol{y}), \boldsymbol{y})\psi_\eta(\boldsymbol{x} - \boldsymbol{y})J(t, \boldsymbol{y})\mathrm{d}\boldsymbol{y}, \tag{3.4}$$

where

$$J = |\det \nabla \tilde{\boldsymbol{q}}^{-1}|, \tag{3.5}$$

up to discretization error.

3.3. Regularized deconvolutions

Define an operator R_η by

$$R_\eta[f](\boldsymbol{x}) = \int \psi_\eta(\boldsymbol{x} - \boldsymbol{y})f(\boldsymbol{y})\mathrm{d}\boldsymbol{y}.$$

To simplify exposition, suppose that R_η is injective. For example, a Gaussian ψ_η produces an injective operator, which is not difficult to check using the Fourier transform and uniqueness of analytic continuation. If R_η is injective, then there exists the single-valued inverse operator R_η^{-1}, that we call the *deconvolution operator*. Unfortunately, this operator is unbounded, since R_η is compact in $L^2(\Omega)$. This is the underlying reason for the popular belief that averaging destroys the high-frequency information contained in the microscopic quantities. In fact, this information is still there (the inverse operator exists), but it is difficult to recover in a stable manner, because of unboundedness. This does not make the situation hopeless, as has been recognized for some time. Reconstructing f from the knowledge of $R_\eta[f]$ is a classical example of an unstable ill-posed problem (small perturbations of the right hand side may produce large perturbations of the solution). The exact

nature of ill-posedness and methods of regularizing the problem are well investigated both analytically and numerically (see, e.g. [9–12,16,8]). Accordingly, we interpret notation R_η^{-1} as a suitable regularized approximation of the exact operator. Many regularizing techniques are currently available: Tikhonov regularization, iterative methods, reproducing kernel methods, the maximum entropy method, the dynamical system approach and others. It is very fortunate that this vast array of knowledge can be used for the ODE model reduction. On the conceptual level, our approach makes it clear that instability associated with ill-posedness is a fundamental difficulty in the process of closing the continuum mechanical equations.

A family of Landweber iterative deconvolution methods [13,14] seems to be particularly convenient in the present context. In the simplest version, approximations g_n to the solution of the operator equation

$$R_\eta[g] = \overline{g}^\eta \tag{3.6}$$

are generated by the formula

$$g_n = \sum_{k=0}^{n} (I - R_\eta)^k \overline{g}^\eta, \qquad g_0 = \overline{g}^\eta. \tag{3.7}$$

The number n of iterations plays the role of the regularization parameter. In (3.7), I denotes the identity operator.

The first three low-order approximations are

$$g_0 = \overline{g}^\eta \quad n = 0, \tag{3.8}$$

$$g_1 = \overline{g}^\eta + (I - R_\eta)[\overline{g}^\eta] \quad n = 1, \tag{3.9}$$

$$g_2 = \overline{g}^\eta + (I - R_\eta)[\overline{g}^\eta] + (I - R_\eta)^2[\overline{g}^\eta] \quad n = 2. \tag{3.10}$$

4. Microscale particle chain equations

In this section, the general method outlined above is detailed in the case of a one-dimensional Hamiltonian chain of oscillators that consists of N identical particles with nearest neighbor interaction. The domain Ω is an interval $(0, L)$. The particle positions, denoted by $q_j = q_j(t), j = 1, \ldots, N$, satisfy

$$0 < q_1 < q_2 < \cdots < q_N < L$$

at all times, i.e. the particles cannot occupy the same position or jump over each other. Next, define a small parameter

$$\varepsilon = \frac{1}{N},$$

and microscale step size

$$h = \frac{L}{N}. \tag{4.1}$$

The interparticle forces

$$f_{jk} = \frac{q_j - q_k}{|q_j - q_k|} U'\left(\frac{|q_j - q_k|}{\varepsilon}\right) \tag{4.2}$$

are defined by a finite range potential U. We suppose that $U'(\xi) \geq 0$ for all ξ within the range. Note that k in (4.2) can take only two values: $j - 1$ or $j + 1$. Also, observe $f_{jk} = -f_{kj}$, as it should be by the third law of Newton, and also that the sign of f_{jk} is the same as the sign of $q_j - q_k$. This means that the force exerted on P_j by say, P_{j+1} is repulsive. The total interaction force acting on the particle P_j is

$$f_j = f_{j,j-1} + f_{j,j+1},$$

for $j = 2, 3, \ldots, N - 1$.

Each particle has mass $m = M/N = M\varepsilon$, where M is the total mass of the system. The particles have velocities denoted by $v_j, j = 1, \ldots, N$. Writing Newton's second law as a system of first order equations yields the scaled microscale ODE system

$$\dot{q}_j = v_j, \qquad \varepsilon M \dot{v}_j = f_j, \quad j = 1, \ldots, N \tag{4.3}$$

subject to the initial conditions

$$q_j(0) = q_j^0, \qquad v_j(0) = v_j^0. \tag{4.4}$$

5. Integral approximation of stresses for particle chains. Mesoscopic continuum equations

In the one-dimensional case stress is a scalar quantity, and (2.10), (2.11) reduce to, respectively,

$$T_{(c)}^\eta(t, x) = -\sum_{j=1}^{N} \frac{M}{N} (v_j - \overline{v}^\eta(t, x))^2 \psi_\eta(x - q_j), \tag{5.1}$$

and

$$T^{\eta}_{(\mathrm{int})}(t,x)=\sum_{j=1}^{N-1}f_{j,j+1}(q_{j+1}-q_j)\int_0^1\psi_\eta(x-sq_{j+1}-(1-s)q_j)\mathrm{d}s. \tag{5.2}$$

The sum in (5.2) is simplified compared to the general expression, since we have exactly $N-1$ interacting pairs of particles.

To obtain integral approximations of the stresses, we define interpolants $\tilde{q}$, $\tilde{v}$, as in Section 3.2. Assuming as before that $\tilde{q}$ is invertible and repeating the calculations we get

$$T^{\eta}_{(c)}(t,x)=-\frac{M}{L}\int_0^L(\tilde{v}(t,y)-\overline{v}^{\eta}(t,x))^2\psi_\eta(x-y)J(t,y)\mathrm{d}y. \tag{5.3}$$

Remark. Many equalities in this paper, including (5.3) hold up to a discretization error. To simplify presentation, we do not mention this in the sequel when discrete sums are approximated by integrals.

The interaction stress can be rewritten as

$$T^{\eta}_{(\mathrm{int})}(t,x)=-\frac{N-1}{N}\sum_{j=1}^{N-1}\frac{L}{N-1}U'\left(\frac{q_{j+1}-q_j}{h}L\right)\frac{q_{j+1}-q_j}{h}\int_0^1\psi_\eta(x-sq_{j+1}-(1-s)q_j)\mathrm{d}s. \tag{5.4}$$

Next we approximate $(q_{j+1}-q_j)/h$ by $\tilde{q}'(t,X_j)$. This approximation is in fact exact, provided the interpolant is chosen to be piecewise linear. Note also that

$$\tilde{q}'(t,X)=\frac{1}{(\tilde{q}^{-1})'(t,\tilde{q}(t,X))}=\frac{1}{J(t,\tilde{q}(t,X))}.$$

Inserting this into (5.4), replacing the Riemann sum with an integral and changing the variable of integration as in Section 3.2, we obtain the integral approximation of the interaction stress:

$$T^{\eta}_{(\mathrm{int})}(t,x)=-\int_0^L U'\left(\frac{L}{J(t,y)}\right)\int_0^1\psi_\eta\left(x-y-\frac{sh}{J(t,y)}\right)\mathrm{d}s\mathrm{d}y. \tag{5.5}$$

Eqs. (5.3), (5.5) contain two microscale quantities: J and $\tilde{v}$. Approximating sums in the definitions of the primary averages (2.6), (2.7) by integrals we see that $\overline{\rho}^{\eta}$ and $\overline{v}^{\eta}$ are obtained by applying the convolution operator R_η to, respectively J and $J\tilde{v}$:

$$\overline{\rho}^{\eta}=\frac{M}{L}R_\eta[J],\qquad \overline{\rho}^{\eta}\overline{v}^{\eta}=\frac{M}{L}R_\eta[J\tilde{v}]. \tag{5.6}$$

The discretization error in (5.6) can be made small by imposing suitable requirements on the microscopic interpolants. Fortunately, the theory of ill-posed problems allows for errors in the right hand side of integral equations. The size of the error determines the choice of regularization parameter. In the present case, the error determines the number of iterations needed for the optimal reconstruction, according to the so-called stopping criteria. These criteria are available in the literature on ill-posed problems (see e.g. [10]). Detailed investigation of these questions is left to future work.

Denote by $R^{-1}_{\eta,n}$ the iterative Landweber regularizing operators

$$R^{-1}_{\eta,n}=\sum_{k=0}^{n}(I-R_\eta)^k.$$

Applying $R^{-1}_{\eta,n}$ in (5.6) yields a sequence of approximations

$$J_n=\frac{L}{M}R^{-1}_{\eta,n}[\overline{\rho}^{\eta}],\qquad \tilde{v}_n=\frac{R^{-1}_{\eta,n}[\overline{\rho}^{\eta}\overline{v}^{\eta}]}{R^{-1}_{\eta,n}[\overline{\rho}^{\eta}]}, \tag{5.7}$$

and a corresponding sequence of closed form mesoscopic continuum equations (written here for an isolated system with zero exterior forces)

$$\partial_t\overline{\rho}^{\eta}+\partial_x(\overline{\rho}^{\eta}\overline{v}^{\eta})=0, \tag{5.8}$$

$$\partial_t(\overline{\rho}^{\eta}\overline{v}^{\eta})+\partial_x(\overline{\rho}^{\eta}(\overline{v}^{\eta})^2)-\partial_x(T^{\eta}_{(c),n}+T^{\eta}_{(\mathrm{int}),n})=0, \tag{5.9}$$

where $T^{\eta}_{(c),n}$, $T^{\eta}_{(\mathrm{int}),n}$ are given by

$$T^{\eta}_{(c),n}=-\frac{M}{L}\int_0^L(\tilde{v}_n(t,y)-\overline{v}^{\eta}(t,x))^2\psi_\eta(x-y)J_n(t,y)\mathrm{d}y, \tag{5.10}$$

$$T^{\eta}_{(\mathrm{int}),n}=-\int_0^L U'\left(\frac{L}{J_n(t,y)}\right)\int_0^1\psi_\eta\left(x-y-\frac{sh}{J_n(t,y)}\right)\mathrm{d}s\mathrm{d}y, \tag{5.11}$$

with J_n, $\tilde{v}_n$ given by (5.7).

6. Zero-order closure for particle chains

Let us consider zero-order approximations in detail. The mesoscopic mesh consists of points

$$x_\beta = \left(\beta - \frac{1}{2}\right)\eta L, \quad \beta = 1, 2, \ldots, B,$$

where $B = 1/\eta$, presumed to be an integer satisfying $B \ll N$. Meso-cells are intervals I_β of length

$$L_\eta = L/B = \eta L,$$

centered at x_β.

Suppose that the only primary variables of interest are density $\overline{\rho}^\eta$ and linear momentum $\overline{\rho}^\eta\overline{v}^\eta$. These variables will be computed by the mesoscale solver. For simplicity, suppose that the meso-solver is explicit in time. Then the average density and average velocity will be available at the previous moment of time. Our task is to design an update step for computing the density and velocity at the next time moment. To construct a closed form update step, we need to approximate the stress T^η in (2.9) in terms of $\overline{\rho}^\eta$, $\overline{\rho}^\eta\overline{v}^\eta$. From the knowledge of $\overline{\rho}^\eta$, $\overline{\rho}^\eta\overline{v}^\eta$ we can approximately recover J and $J\tilde{v}$. The zero-order approximation (3.8) corresponds to

$$J(t,x) \approx \frac{L}{M}\overline{\rho}^\eta(t,x), \tag{6.1}$$

$$J(t,x)\tilde{v}(t,x) \approx \frac{L}{M}\overline{\rho}^\eta\overline{v}^\eta(t,x). \tag{6.2}$$

In other words, the microscale quantities are approximated by their averages. The corresponding closed form approximations for stress are obtained by inserting (6.1), (6.2) into (5.10), (5.11):

$$T^\eta_{(c),0}(t,x) = -\int_0^L (\overline{v}^\eta(t,y) - \overline{v}^\eta(t,x))^2\psi_\eta(x-y)\overline{\rho}^\eta(t,y)\mathrm{d}y, \tag{6.3}$$

$$T^\eta_{(\mathrm{int}),0} = -\int_0^L U'\left(\frac{M}{\overline{\rho}^\eta(t,y)}\right)\int_0^1 \psi_\eta\left(x - y - \frac{shM}{L\overline{\rho}^\eta(t,y)}\right)\mathrm{d}s\mathrm{d}y. \tag{6.4}$$

For computation, a numerical quadrature should be used. In this regard, note that all average quantities are computed on the mesoscale mesh, while the formulas (2.10), (2.11) are fine scale discretizations. Therefore, one might wonder if a straightforward mesoscale quadrature of (6.3), (6.4) is too crude. A better approach is to interpolate $\overline{\rho}^\eta$, $\overline{v}^\eta$ by prescribing approximate particle positions $\hat{q}_j$ and velocities $\hat{v}_j$, $j = 1, 2, \ldots, N$, compatible with the given $\overline{\rho}^\eta$, $\overline{v}^\eta$. Once this is done, (6.3), (6.4) can be discretized on a fine scale mesh with mesh nodes $\hat{q}_j$.

Interpolants cannot be unique. For zero-order closure, we are choosing positions and velocities that produce the given average density and average velocity. Clearly, there are many different position-velocity configurations with the same averages. The choice made in this paper is motivated by the practical requirement of achieving a low operation count, as well as by certain expectations about the nature of dynamics. From the continuum mechanical point of view, if a system can be adequately modeled by balance equations of mass and momentum, then it must have have a trivial energy balance. Most often this means that the deformation is nearly isothermal. To mimic such isothermal dynamics we suppose that at each time step, there exists a positive number κ^2 (it can be called the "upscaling temperature") such that

$$\sum_{j\in J_\beta}(v_j^\beta - \overline{v}^\eta(t,x_\beta))^2\psi_\eta(x_\beta - \hat{q}_j) = \kappa^2. \tag{6.5}$$

Here the summation is over all particles located in a meso-cell I_β. The temperature κ^2 is the same for all $\beta = 1, 2, \ldots, B$. We emphasize that *the actual value* of κ^2 is not as important as the fact that its value is the same for all meso-cells. This is because (6.5) would yield constant mesoscale mesh node values of $T^\eta_{(c),0}$ As a result, the finite difference approximation of $\partial_x T^\eta_{(c),0}$ on the mesoscale mesh is identically zero. We interpret this by saying that convective stress does not contribute to the mesoscopic dynamics in the isothermal case. Another observation is that κ need not be the same at different moments of time, so our assumption is somewhat more flexible than the standard isothermal deformation approximation. Also, we note that validity (6.5) depends on the choice of η. For bigger η, it is more likely that (6.5) holds for the same underlying microscopic dynamics. Details on this are provided below in Section 6.2. Additionally, other features of the microscopic dynamics should be taken into account. Most importantly, the interpolated velocities $\hat{v}_j = \overline{v}^\eta(\hat{q}_j)$ must be such that the collection $\hat{q}_j, \hat{v}_j, j = 1, 2, \ldots, N$ conserves microscopic energy $\mathcal{E}$:

$$\mathcal{E} = \frac{1}{2}\frac{M}{N}\sum_{j=1}^N(\hat{v}_j)^2 + \mathcal{U}(\widehat{Q}) \tag{6.6}$$

where $\mathcal{U}(\widehat{Q})$ is the microscale potential energy corresponding to the positions $\hat{q}_j$.

6.1. Prescribing particle positions

The objective of this section is to assign approximate particle positions $\hat{q}_j$. We start by interpolating J. The simplest interpolant is piecewise-constant: $J(t,\boldsymbol{x}) \approx \sum_{\beta=1}^{B} J(t,x_\beta)\chi_\beta(\boldsymbol{x}) = \sum_{\beta=1}^{B} \frac{L}{M}\overline{\rho}^\eta(t,x_\beta)\chi_\beta(\boldsymbol{x})$ where χ_β is the characteristic function of the meso-cell I_β. A simple choice of the position map compatible with this interpolant is a piecewise linear map having the prescribed constant value of J in each meso-cell. In practical terms, this means that in each meso-cell, particles are spaced at equal intervals from each other. The local interparticle spacing

$$\Delta_\beta = \frac{M}{\overline{\rho}^\eta(t,x_\beta)N} \tag{6.7}$$

is determined by the mesh value of the average density. To explain (6.7), note that the total mass of particles contained in the meso-cell I_β can be approximated by $\overline{\rho}^\eta(t,x_\beta)L_\eta$. Dividing by the mass M/N of one particle, we obtain an approximate number of particles inside I_β:

$$n_\beta = \overline{\rho}^\eta(t,x_\beta)L_\eta\frac{N}{M},$$

and thus $\Delta_\beta = L_\eta/n_\beta$. We emphasize that $\hat{q}_j$ are chosen based only on the known mesh values of the density $\overline{\rho}^\eta$, and that $\hat{q}_j$ will be different from the actual particle positions q_j.

Now we approximate the integral in (6.4) by its Riemann sum generated by the partition $\{\hat{q}_j, j = 1, 2, \ldots, N\}$:

$$T^\eta_{(\mathrm{int}),0} \approx -\sum_{j=1}^{N-1} U'(N(\hat{q}_{j+1}-\hat{q}_j))(\hat{q}_{j+1}-\hat{q}_j)\int_0^1 \psi_\eta(x - s\hat{q}_{j+1} - (1-s)\hat{q}_j)\mathrm{d}s. \tag{6.8}$$

6.2. Prescribing particle velocities

In order to approximate the convective stress in the fine scale discretization of (6.3), we need to choose approximations $\hat{v}_j$ of the true particle velocities v_j. The choice of $\hat{v}_j$ must satisfy (6.6) and be compatible with the available average velocity at the mesoscale mesh nodes.

For each $\hat{q}_j \in I_\beta$, we set

$$\hat{v}_j = \overline{v}^\eta_\beta + \delta v^\beta_j,$$

where $\overline{v}^\eta_\beta$ is the local average velocity, and δv^β_j is a perturbation to be defined.

Next, we show that the energy-conserving collection of δv_j velocity always exists, provided its upscaling temperature is suitably prescribed. This prescription will be based only on the available mesoscale information. For definitiveness, in the rest of this section we suppose that ψ_η satisfies the following condition:

$$\psi_\eta(x_\beta - \hat{q}_j) > 0, \quad \text{if } \hat{q}_j \in I_\beta. \tag{6.9}$$

To make the algebra simpler, we make another assumption: for each $\beta = 1, 2, \ldots, B$,

$$\sum_{j=1}^{N} f(\hat{v}_j)\psi_\eta(x_\beta - \hat{q}_j) \approx \sum_{j\in J_\beta} f(\hat{v}_j)\psi_\eta(x_\beta - \hat{q}_j), \tag{6.10}$$

where f is either $\hat{v}_j$ or $(\hat{v}_j)^2$. The second summation is over all j such that $\hat{q}_j \in I_\beta$. Assumption (6.10) holds when $\psi_\eta(x_\beta - y)$ is small outside of I_β.

Averaging of $\hat{v}_j$ should produce the known average velocity $\overline{v}^\eta_\beta$. This yields an equation for δv_j:

$$\frac{M}{N}\sum_{j\in J_\beta}\hat{v}_j\psi_\eta(x_\beta - \hat{q}_j) = \overline{\rho}^\eta_\beta\overline{v}^\eta_\beta. \tag{6.11}$$

Since

$$\begin{aligned}\frac{M}{N}\sum_{j\in J_\beta}\hat{v}_j\psi_\eta(x_\beta - \hat{q}_j) &= \overline{v}^\eta_\beta\frac{M}{N}\sum_{j\in J_\beta}\psi_\eta(x_\beta - \hat{q}_j) + \frac{M}{N}\sum_{j\in J_\beta}\delta v^\beta_j\psi_\eta(x_\beta - \hat{q}_j)\\ &= \overline{\rho}^\eta_\beta\overline{v}^\eta_\beta + \frac{M}{N}\sum_{j\in J_\beta}\delta v^\beta_j\psi_\eta(x_\beta - \hat{q}_j),\end{aligned}$$

(6.11) holds provided

$$\frac{M}{N}\sum_{j\in J_\beta}\delta v_j^\beta \psi_\eta(x_\beta-\hat{q}_j)=0. \tag{6.12}$$

Now we look for perturbations in the form

$$\delta v_j^\beta=\frac{a_j^\beta}{\psi_\eta(x_\beta-\hat{q}_j)}, \tag{6.13}$$

where the a_j^β are to be determined. Next, narrow down the choice of a_j^β by setting

$$a_j^\beta=t\tilde{a}_j^\beta, \tag{6.14}$$

where $\tilde{a}_j^\beta$ is either one or negative one. To satisfy (6.12) we need n_β to be even (one more point can be easily inserted if the actual n_β is odd); in addition, the number of positive and negative $\tilde{a}_j^\beta$ must be the same.

To simplify further calculations, we write conservation of energy (6.6) in the form

$$\sum_{j\in J_\beta}(\delta v_j^\beta)^2=K_\beta, \tag{6.15}$$

where K_β are any numbers satisfying

$$K_\beta>0,\quad \sum_{\beta=1}^{B}K_\beta=\frac{2N}{M}\left(\mathcal{E}-\mathcal{U}(\widehat{Q})-\frac{1}{2}\frac{M}{N}\sum_{\beta=1}^{B}(\overline{v}_\beta^\eta)^2 n_\beta\right). \tag{6.16}$$

Our goal now is to show that there is a choice of K_β, $\hat{\kappa}^2$ and t such that δv_j^β defined by (6.13), (6.14) satisfy Eqs. (6.5), (6.15), and (6.16). Inserting (6.13) into (6.5) and (6.15) yields, respectively,

$$t^2\sum_{j\in J_\beta}\frac{1}{\psi_\eta(x_\beta-\hat{q}_j)}=\hat{\kappa}^2, \tag{6.17}$$

$$t^2\sum_{j\in J_\beta}\frac{1}{(\psi_\eta(x_\beta-\hat{q}_j))^2}=K_\beta. \tag{6.18}$$

Combining these equations we get

$$t^2=\hat{\kappa}^2\left(\sum_{j\in J_\beta}\frac{1}{\psi_\eta(x_\beta-\hat{q}_j)}\right)^{-1}, \tag{6.19}$$

$$\hat{\kappa}^2\sum_{j\in J_\beta}\frac{1}{(\psi_\eta(x_\beta-\hat{q}_j))^2}\left(\sum_{j\in J_\beta}\frac{1}{\psi_\eta(x_\beta-\hat{q}_j)}\right)^{-1}=K_\beta. \tag{6.20}$$

Substituting into (6.16) yields the choice of $\hat{\kappa}$:

$$\hat{\kappa}^2=\frac{2N}{M}\left(\mathcal{E}-\mathcal{U}(\widehat{Q})-\frac{1}{2}\frac{M}{N}\sum_{\beta=1}^{B}(\overline{v}_\beta^\eta)^2 n_\beta\right)\left(\sum_{\beta=1}^{B}\frac{\sum_{j\in J_\beta}\frac{1}{(\psi_\eta(x_\beta-\hat{q}_j))^2}}{\sum_{j\in J_\beta}\frac{1}{\psi_\eta(x_\beta-\hat{q}_j)}}\right)^{-1}. \tag{6.21}$$

The choice of all constants now should be made as follows:

(1) Given $\mathcal{E}$, $\overline{v}_\beta^\eta$, $\hat{q}_j$, find $\hat{\kappa}$ by (6.21);
(2) Determine K_β from (6.20);
(3) Determine t from (6.19);
(4) Choose δv_j^β by (6.13), (6.14).

Note that step 4 introduces non-uniqueness, but we are concerned only with the existence of suitable velocity perturbations. The actual choice of δv_j^β will not change the mesoscopic discretization of the momentum balance equation. Indeed, once $\hat{q}_j$, $\hat{v}_j$ are chosen, we can approximate the integral in (6.3) (for x at the mesoscale mesh nodes) by a Riemann sum corresponding to the partition $\hat{q}_j$ of $(0, L)$:

$$\begin{aligned} T^\eta_{(c),0}(t, x_\alpha) &= -\sum_{\beta=1}^{B} \sum_{j\in J_\beta} \frac{L_\eta}{n_\beta} (\delta v_j^\beta)^2 \psi_\eta(x_\alpha - \hat{q}_j)\overline{\rho}^\beta \\ &= -\sum_{j\in J_\alpha} (\delta v_j^\alpha)^2 \psi_\eta(x_\alpha - \hat{q}_j) \\ &= -\hat{\kappa}^2, \quad \alpha = 1, 2, \ldots, B. \end{aligned} \tag{6.22}$$

Therefore, the mesoscale mesh values of $T^\eta_{(c),0}$ are all equal. This implies that a finite difference approximation of $\partial_x T^\eta_{(c),0}$ on the mesoscale mesh vanishes. The conclusion is that for isothermal dynamics, any suitable choice of a velocity perturbation produces a convective stress that has zero divergence on the mesoscale.

6.3. Zero-order isothermal continuum model

Combining the approximation $\partial_x T^\eta_{(c),0} = 0$ with (6.3), (6.4) we obtain an isothermal zero-order continuum model

$$\partial_t \overline{\rho}^\eta + \partial_x(\overline{\rho}^\eta \overline{v}^\eta) = 0, \tag{6.23}$$

$$\partial_t(\overline{\rho}^\eta \overline{v}^\eta) + \partial_x(\overline{\rho}^\eta (\overline{v}^\eta)^2) - \partial_x T^\eta_{(\mathrm{int}),0} = 0, \tag{6.24}$$

where $T^\eta_{(\mathrm{int}),0}$ is given by an integral expression (6.4) (or by a discretization (6.8)). We can interpret the interaction stress as pressure. Then (6.4) provides the dependence of pressure on density, which is non-local in space and non-linear. For small h (large N), it can be approximated by

$$T^\eta_{(\mathrm{int}),0} \approx -\int_0^L U'\left(\frac{M}{\overline{\rho}^\eta(t, y)}\right) \psi_\eta(x - y)\mathrm{d}y,$$

which is still non-local. In the limiting case $\eta \to 0$, observing that convolution with ψ_η is an approximate identity, this equation can be reduced to a local equation of state

$$T^\eta_{(\mathrm{int}),0} \approx -U'\left(\frac{M}{\overline{\rho}^\eta(t, x)}\right).$$

If $\overline{\rho}^\eta$ is nearly constant, this equation can be linearized to produce a classical gas dynamics linear equation of state. This shows that zero-order closure (6.4) generalizes several classical phenomenological equations of state. The connection between micro- and mesoscales is made explicit in (6.4). Using higher order closure approximations, one can obtain other non-classical continuum models worth further investigation.

7. Computational results

In this section, the method developed in the previous sections is tested for a chain of $N = 10{,}000$ to $N = 80{,}000$ particles interacting with a non-linear finite range potential

$$U(\xi) = \begin{cases} C_r\left(\frac{1}{1-p}\xi^{1-p}x_\star - \xi x_\star^{1-p} + \frac{p}{p-1}x_\star^{2-p}\right), & \text{if } \xi \in (0, x_\star] \\ 0, & \text{if } \xi > x_\star \end{cases} \tag{7.1}$$

where $p > 1$, $x_\star = \alpha L$, $\alpha \approx 1$ and C_r is material stiffness. This potential mimics a Hertz potential used in the modeling of granular media. Particles in this model are centers of lightly touching spherical granules arranged in a chain, and the ODEs model acoustic wave propagation in this chain. The microscale equations are (4.3), (4.4) with initial conditions given below. The forces include the pair interaction forces defined by U, and the exterior confining forces acting on the first and last particles. The parameters of U are chosen so that all particles stay within the interval $[0, L]$ for the duration of a simulation. To ensure that particles do not leave the interval $[0, L]$, its endpoints are modeled as stationary particles that interact with the moving particles with forces generated by the same potential U. If needed, the stiffness of the walls can be increased by using a different value of C_r.

Let x_β be the centers of the mesocells I_β, $\beta = 1, 2, \ldots, B$, as defined in Section 6. Next, let a window function $\psi(x)$ be the characteristic function of the interval $[-\frac{1}{2}\eta L, \frac{1}{2}\eta L)$. The average density and momentum are defined by (2.6) and (2.7),

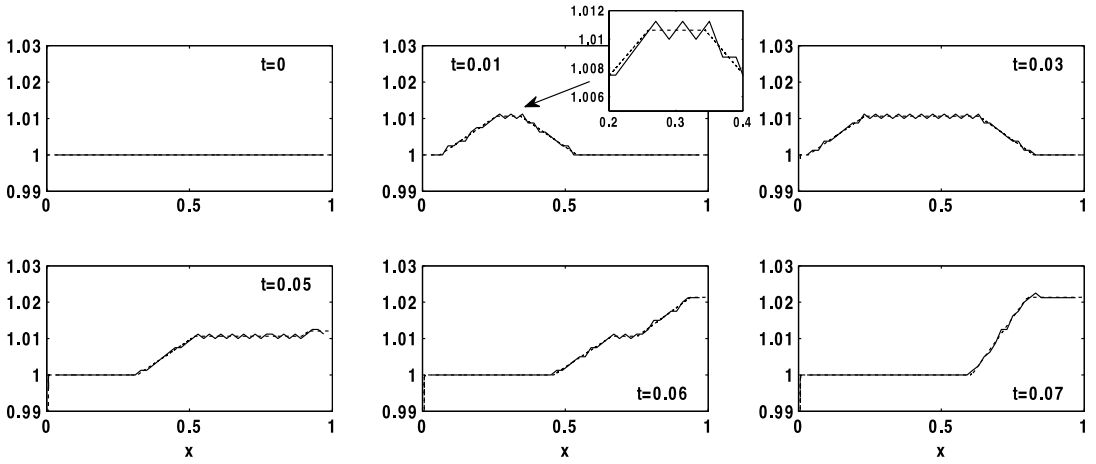

Fig. 1. $N = 40{,}000$, $B = 50$. Dashed line: Jacobian $J(t, x_\beta)$; solid line: its mesoscale approximation $\frac{L}{M}\overline{\rho}^\eta(t, x_\beta)$, $\beta = 1, 2, \ldots, B$ according to (6.1). The blowup of the results at $t = 0.01$ shows the discrepancy between $J(t, x_\beta)$ and $\frac{L}{M}\overline{\rho}^\eta(t, x_\beta)$.

respectively, and the average velocity is

$$\overline{v}_\beta(t) = \frac{\sum_{j=1}^{N} v_j(t)\psi(x_\beta - q_j(t))}{\sum_{j=1}^{N} \psi(x_\beta - q_j(t))}.$$

The average density $\overline{\rho}^\eta$ evaluated at the center x_β of a mesocell I_β can be written as

$$\overline{\rho}^\eta_\beta(t) = \overline{\rho}^\eta(t, x_\beta) = \frac{M}{N}\sum_{j=1}^{N}\frac{1}{\eta L}\psi\left(\frac{x_\beta - q_j(t)}{\eta}\right) = \frac{B}{N}\frac{M}{L}\sum_{j=1}^{N}\psi\left(\frac{x_\beta - q_j(t)}{\eta}\right). \tag{7.2}$$

We solve microscopic equations (4.3), (4.4) subject to the initial positions

$$q_j^0 = \left(j - \frac{1}{2}\right)h, \quad j = 1, 2, \ldots, N, \ h = \frac{L}{N},$$

and the initial velocities

$$v_j^0 = \begin{cases} \gamma, & \text{if } 0 \le q_j^0 \le \dfrac{L}{5}, \\ \gamma\left(-\dfrac{5}{L}q_j^0 + 2\right), & \text{if } \dfrac{L}{5} \le q_j^0 \le \dfrac{2L}{5}, \\ 0, & \text{if } \dfrac{2L}{5} \le q_j^0 \le L \end{cases}$$

using the Velocity Stormer–Verlet method. We use $L = 1, p = 2, \alpha = 1, \gamma = 0.3$ and $C_r = 100$. This velocity profile initiates an acoustic wave that propagates to the right. The stiffness constant C_r can be used to ensure that particles have only small displacements from their equilibrium positions. Using an initial velocity with higher γ would require a higher value of C_r to enforce the smallness of typical particle displacements.

We integrate microscopic equation (4.3), (4.4) until the acoustic wave reaches the right wall, interacts with it and is about of being reflected to the left, which corresponds to $t = 0.07$. To capture the most interesting dynamics, we present snapshots of the results at times $t = 0, 0.01, 0.03, 0.05, 0.06$ and 0.07. To test our closure method, we compute the microscopic positions q_j and velocities $v_j, j = 1, \ldots, N$, at every time step and use them to evaluate the primary mesoscopic variables: average density $\overline{\rho}^\eta_\beta$ and average velocity $\overline{v}^\eta_\beta$, at the mesocell centers x_β, $\beta = 1, \ldots, B$. These mesoscopic quantities are defined in (2.6), (2.7) (see also (5.6)). They are then employed in computing the zero-order approximation $T^\eta_{(\mathrm{int}),0}(t, x_\beta)$ defined in (6.4). We compare this mesoscopic approximation with the "exact" microscopic interaction stress $T^\eta_{(\mathrm{int})}(t, x_\beta)$ defined in (5.2), and also test other approximations given by (6.1), (6.2).

Comparing $v_j, j = 1, \ldots, N$ and $\overline{v}^\eta_\beta, \beta = 1, 2, \ldots, B$ (not shown here) we find that micro- and mesoscale velocities are essentially indistinguishable during the simulation time.

In Fig. 1, we analyze microscopic Jacobian $J(t, x_\beta)$ together with its zero-order mesoscopic approximation $\frac{L}{M}\overline{\rho}^\eta(t, x_\beta)$ obtained according to (6.1). In this and other figures, we plot "exact" microscopic quantities using a dashed line while

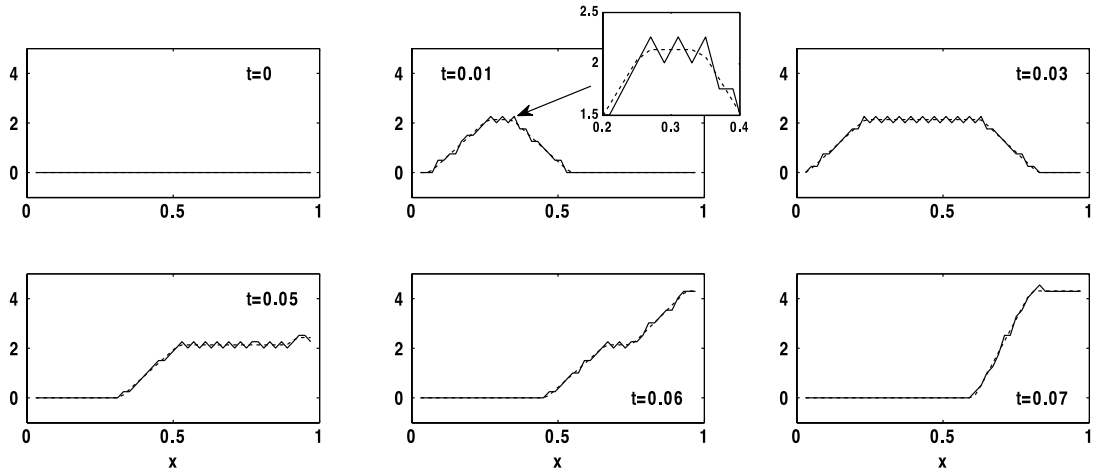

Fig. 2. $N = 40{,}000$, $B = 50$. Dashed line: exact interaction stress $T^{\eta}_{(\mathrm{int})}(t, x_\beta)$; solid line: its approximation $T^{\eta}_{(\mathrm{int}),0}(t, x_\beta)$, $\beta = 1, 2, \ldots, B$, defined in (6.4). The blowup of the results at $t = 0.001$ shows the difference between the exact stress and its approximation.

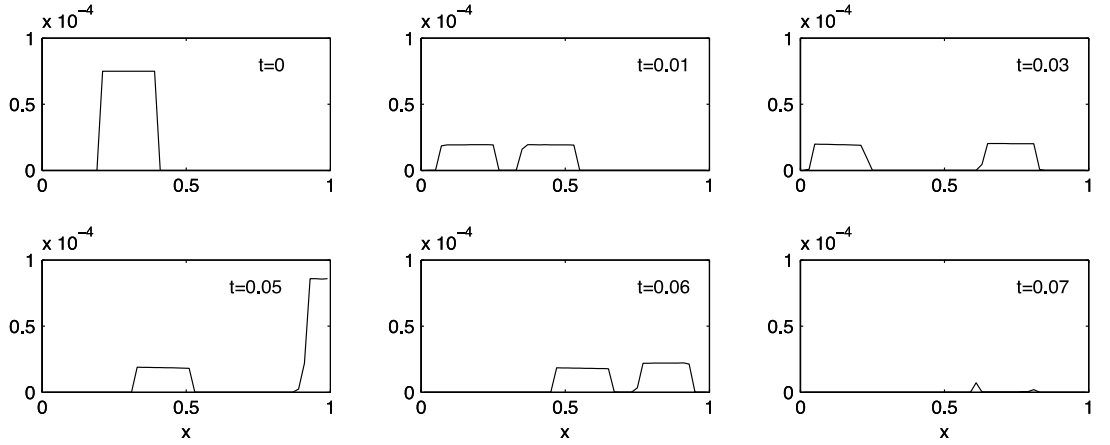

Fig. 3. $N = 40{,}000$, $B = 50$. Convective stress $T^{\eta}_{(c)}(t, x_\beta)$, $\beta = 1, 2, \ldots, B$, defined in (6.3).

mesoscopic quantities are depicted with a solid line. The results shown in Fig. 1 indicate that $\frac{L}{M}\overline{\rho}^{\eta}(t, x_\beta)$ exhibits some oscillations whose amplitude is about 10^{-3} as compared to Jacobian $J(t, x_\beta)$. The oscillations are likely caused by the choice of a window function ψ. For computational testing, we chose ψ to be a characteristic function. The main reason was to try "the worst case scenario" concerning the smoothness of ψ. We expected that this window function would produce more oscillations than a smoother ψ. A good agreement between our approximation and the direct simulation results strongly suggest that the proposed method is viable. We believe that it should perform better with a smoother choice of ψ. The oscillations present in $\frac{L}{M}\overline{\rho}^{\eta}(t, x_\beta)$ are amplified in the approximated stress $T^{\eta}_{(\mathrm{int}),0}(t, x_\beta)$, due to the rather high stiffness constant $C_r = 100$, as shown in Fig. 2. We also compare microscopic $J(t, x_\beta)\tilde{v}(t, x_\beta)$ with its zero-order approximation $\frac{L}{M}\overline{\rho}^{\eta}(t, x_\beta)\overline{v}^{\eta}(t, x_\beta)$ according to (6.2). Graphs are not shown here but we find that these quantities agree very well similar to micro- and mesoscale velocities. Finally, we verify that the dynamics is quasi-isothermal by plotting the convective stress $T^{\eta}_{(c)}(t, x_\beta)$ defined in (5.11) in Fig. 3. As can be seen, the fluctuations in the convective stress do not exceed 10^{-4} throughout the computational time, therefore, the kinetic energy of the velocity fluctuations is small.

We next tested the effect of the scale separation on the quality of the zero-order approximation. With fixed $B = 50$, we allowed N to vary from 10,000 to 80,000 and followed the evolution of mesoscale quantities of interest: $\frac{L}{M}\overline{\rho}^{\eta}(t, x_\beta)$ and $T^{\eta}_{(\mathrm{int}),0}(t, x_\beta)$. Snapshots of these functions at the same representative time $t = 0.01$ are plotted in Figs. 4 and 5, respectively, with $N = 10{,}000$, $N = 20{,}000$ and $N = 80{,}000$. The results with $N = 40{,}000$ at the same time are given the middle top panels in Figs. 1, 2 for comparison. It is clear that as the scale separation increases, the oscillations in both $\frac{L}{M}\overline{\rho}^{\eta}(t, x_\beta)$ and $T^{\eta}_{(\mathrm{int}),0}(t, x_\beta)$ diminish and when $N = 80{,}000$, the exact microscopic quantities and their mesoscale approximations are almost indistinguishable.

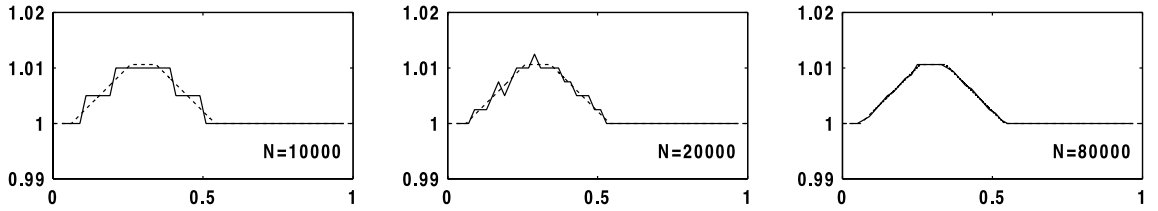

Fig. 4. Effect of the scale separation on $\frac{L}{M}\overline{\rho}^{\eta}$. $B = 50$ is fixed, N varies, data is taken at the same $t = 0.01$. Dashed line: Jacobian $J(t, x_\beta)$; solid line: its mesoscale approximation $\frac{L}{M}\overline{\rho}^{\eta}(t, x_\beta)$, $\beta = 1, 2, \ldots, B$.

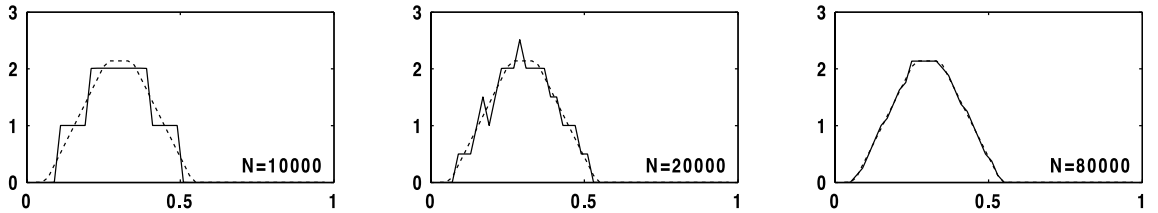

Fig. 5. Effect of the scale separation on $T^{\eta}_{(\mathrm{int}),0}$. $B = 50$ is fixed, N varies, data is taken at the same $t = 0.01$. Dashed line: exact interaction stress $T^{\eta}_{(\mathrm{int})}(t, x_\beta)$; solid line: its mesoscale approximation $T^{\eta}_{(\mathrm{int}),0}(t, x_\beta)$, $\beta = 1, 2, \ldots, B$.

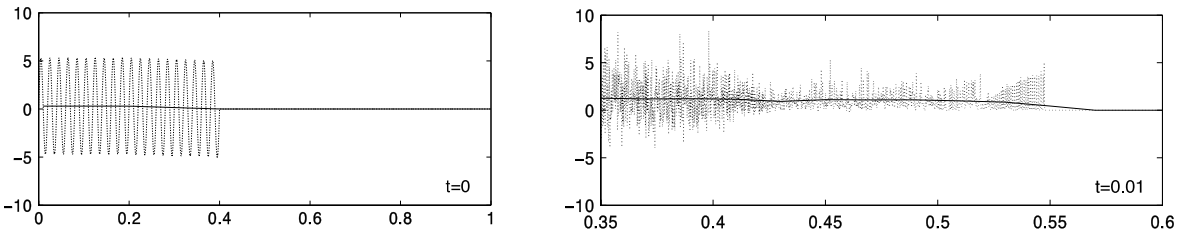

Fig. 6. Example with imposed high frequency oscillations. $N = 10{,}000$, $B = 50$. Dashed line: exact velocity $v_j, j = 1, 2, \ldots, N$; solid line: average velocity $\overline{v}_\beta, \beta = 1, 2, \ldots, B$.

In the above example, the fluctuations of microscopic velocities about their average values were very small and the zero-order approximation worked well. Next we show that if microscopic velocities have high fluctuations then the zero-order approximation is not capable of captioning an appropriate dynamics.

We demonstrate this by imposing high frequency k oscillations with a relatively large amplitude a on the nonzero portion of the initial velocity used in the previous experiments. The initial velocity is

$$v_j^0 = \begin{cases} \gamma + a \sin\left(\dfrac{5k\pi}{L} q_j^0\right), & \text{if } 0 \le q_j^0 \le \dfrac{L}{5}, \\ \gamma\left(-\dfrac{5}{L} q_j^0 + 2\right) + a \sin\left(\dfrac{5k\pi}{L} q_j^0\right), & \text{if } \dfrac{L}{5} \le q_j^0 \le \dfrac{2L}{5}, \\ 0, & \text{if } \dfrac{2L}{5} \le q_j^0 \le L \end{cases}$$

and it is plotted in the left panel of Fig. 6. We use $a = 5$ and $k = 20$ which gives one period of imposed oscillations per mesocell. This microscopic initial velocity has a property that the average velocity at time $t = 0$ is exactly the same as in the previous example. Simulations were done with $N = 10{,}000$ until the same $t = 0.07$.

The right panel of Fig. 6 shows a typical microscopic velocity profile together with its average velocity (taken at $t = 0.01$): to the left from the wave front, the microscopic velocity has large frequency oscillations (due to dispersion?) with an amplitude sometimes exceeding the initial amplitude by a factor of 1.5 and to the right from the wave front, the microscopic velocity is zero. Clearly, the average velocity is very different from the microscopic velocity.

Analysis of the microscopic Jacobian $J(t, x_\beta)$ and mesoscopic $\frac{L}{M}\overline{\rho}^{\eta}(t, x_\beta)$ reveals that these functions have qualitatively the same dynamics as the micro- and mesoscale velocities, respectively, shown in Fig. 6. We plot the former in Fig. 7 where the left panel has graphs at $t = 0$ while the right panel shows a typical structure with data taken at $t = 0.01$. It is interesting to note that the zero-order approximation $T^{\eta}_{(\mathrm{int}),0}(t, x_\beta)$ to the interaction stress $T^{\eta}_{(\mathrm{int})}(t, x_\beta)$ plotted in Fig. 8 does not agree in those areas that were affected by large magnitude oscillations in microscopic velocities while it agrees well in those areas to which oscillations have not come yet. This finding suggests that the zero-order approximation should not be used for large frequency oscillations in microscopic velocities and a higher order approximation is needed.

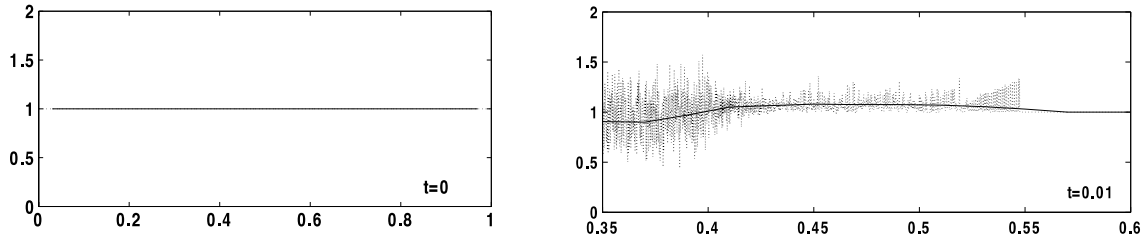

Fig. 7. Example with imposed high frequency oscillations. $N = 10{,}000$, $B = 50$. Dashed line: Jacobian $J(t, x_\beta)$; solid line: its mesoscale approximation $\frac{L}{M}\overline{\rho}^\eta(t, x_\beta)$, $\beta = 1, 2, \ldots, B$ (compare with Fig. 1).

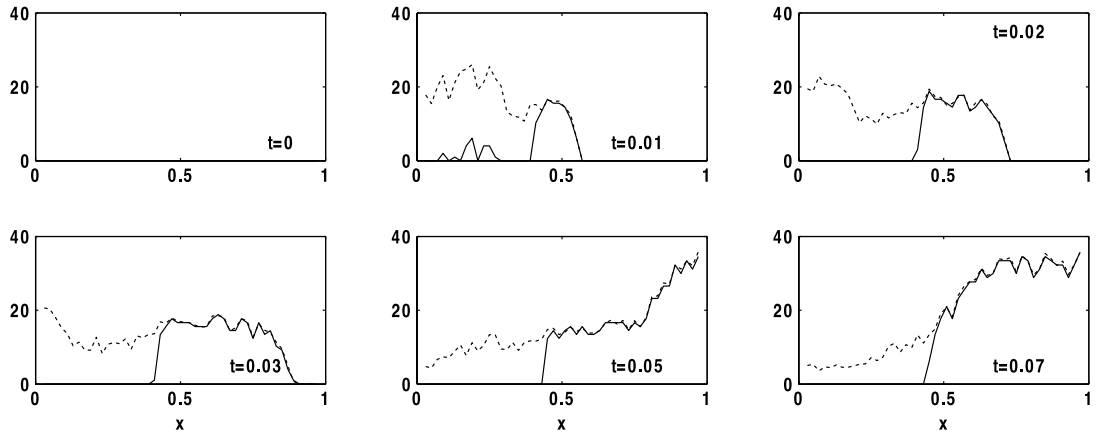

Fig. 8. Example with imposed high frequency oscillations. $N = 10{,}000$, $B = 50$. Dashed line: exact interaction stress $T^\eta_{(\mathrm{int})}(t, x_\beta)$; solid line: its mesoscale approximation $T^\eta_{(\mathrm{int}),0}(t, x_\beta)$ (compare with Fig. 2).

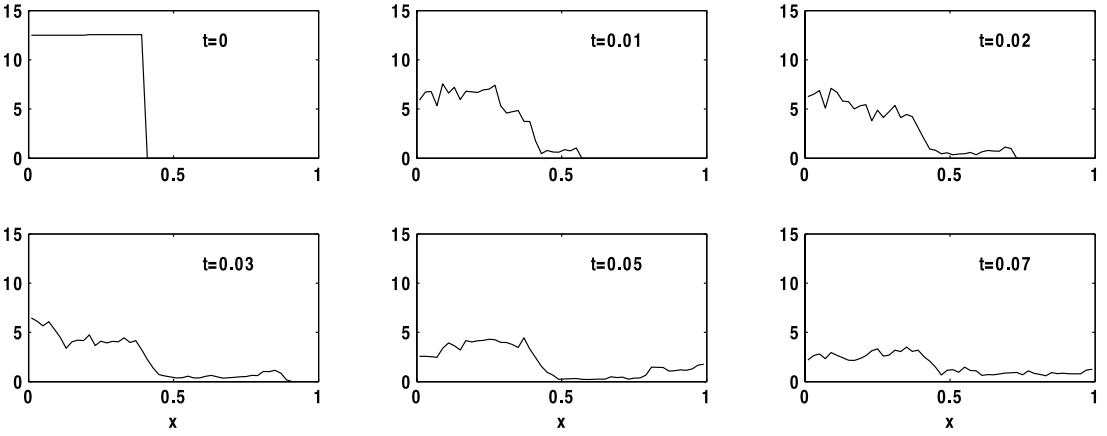

Fig. 9. Example with imposed high frequency oscillations. $N = 10{,}000$, $B = 50$. Convective stress $T^\eta_{(c)}(t, x_\beta)$, $\beta = 1, 2, \ldots, B$ (compare with Fig. 3).

Finally, in Fig. 9 we plot the convective stress $T^\eta_{(c)}(t, x_\beta)$ whose large values confirm that the oscillations in microscopic velocities are much bigger during the computational time than those in the first example. When the initial velocity has fluctuations with a frequency higher than $k = 20$, the discrepancy between micro- and mesoscale quantities is even more pronounced.

8. Zero-order closure: applicability

Zero-order closure is very similar to the use of the Cauchy–Born rule in quasi-continuum simulations of solids. Here, the nodes of the mesoscale mesh can be thought of as "representative particles". These particles are moved with the average velocity, while the velocities of other particles are assigned by interpolation. A construction of an interpolant should take into account the physics of the microscopic model such as energy conservation. In the computational example of Section 7, the

zero-order approximation turns out to be quite accurate, when non-oscillatory initial conditions are imposed. In this case, we found that the approximate and exact stresses agree rather well, and this agreement becomes better with increasing scale separation. This does not mean that zero-order closure always works well. Our numerical simulations suggest that the applicability of zero-order closure is determined by initial conditions, exterior forces and interaction potential (arranged in order of importance).

Approximating functions by their averages we neglect fluctuations. Therefore, the initial velocities should have small fluctuations. The initial positions should be chosen so that the number of particles in a meso-cell varies slightly from one cell to another. The initial velocity fluctuations in our first example are small, and the convective stress at later times is by three orders of magnitude smaller than the interaction stress. This remains true on the time interval sufficient for the traveling wave to reach the opposite end of the chain.

For one-dimensional problems, convective stress is proportional to the kinetic energy of velocity fluctuations. This kinetic energy can be naturally associated with the upscaling temperature. The relative smallness of the convective stress means that the upscaling temperature is nearly zero. Therefore, the corresponding dynamics can be termed *cold*. We also note that cold dynamics is a special case of isothermal dynamics, considered in Section 6. As has been remarked earlier, isothermal dynamics implies that divergence of the convective stress is nearly zero on the mesoscale, and thus can be neglected compared with the divergence of the interaction stress.

Another consideration is related to inhomogeneity in actual particle distribution. In our example, deviations of about 4% in relative particle positions produced visible oscillations in the approximation of the interaction stress. This amplification of small perturbations is due to the stiffness of the interaction potential. However, the same stiffness prevents particle aggregation, keeping the interparticle distances bounded from below. Bounds from above are difficult to enforce with the chosen potential because it does not have a potential well. An isolated particle system with this potential would just fall apart. This phenomenon is commonplace for granular materials. The particles remain confined to the domain (container) only because they are repelled by the walls. Walls have very little direct influence on the interparticle distances in the systems' interior. Therefore, the applicability of zero-order closure also depends on the stiffness of the problem, and more generally on how well the potential enforces uniform particle distribution. In that sense, zero-order closure makes a reasonable approximation for lattice systems modeling small deformation of solids at constant temperature.

To further understand the limitations of zero-order closure, consider the effect of increasing the order n of the Landweber approximations (3.7). The Fourier transform the kernel of $I - R_\eta$ with Gaussian ψ_η is equal to

$$1 - \mathrm{e}^{-\eta^2\pi^2\xi\cdot\xi}.$$

It is very small for ξ close to zero, and then increases to one as $|\xi|$ goes to infinity. Therefore, $I - R_\eta$ acts as a filter damping low frequencies and thus emphasizing the higher frequency content of the signal. Higher order approximations amount to applying convolutions $\sum_{k=1}^{n}(I-R_\eta)^k$ to mesoscale averages. As n increases, the high frequency content of the reconstruction will be increasingly amplified. This suggests that systems capable of producing large fluctuations should be handled with higher order approximations.

A related comment is that averages of fluctuations can become additional state variables in a mesoscale continuum model. A familiar example is the use of the averaged energy balance equation (see [1] for derivation), in addition to the mass and momentum balance. The energy balance equation describes the evolution of the density of kinetic energy of velocity fluctuations. An intriguing question here is how the model with just two equations of balance but high order closure approximation compares with a zero-order closure model containing all three balance equations. In classical physics, additional balance equations are often introduced as a means of compensating for errors introduced by replacing state variables with their averages. The use of higher order closure could offer an alternative to this approach. Indeed, suppose that one is interested only in tracking density and velocity on the mesoscale. The corresponding two balance equations contain only two microscale quantities: the velocity field $\tilde{v}$ and the Jacobian J of the inverse position map $\tilde{q}^{-1}$. If $\tilde{v}$ and J can be accurately reconstructed from their averages, we do not need to deal with the energy balance equation. This observation offers a new way of reducing the computational cost. Higher order approximations are more expensive than zero-order, but using more balance equations also increases the computational cost. We also note that increasing the order of closure approximations involves repeated convolutions with the window function ψ_η. On the other hand, simulating an energy balance involves numerical integration of an additional non-linear integral–differential equation, a much more difficult task.

9. Conclusions

We propose a closure method that gives closed form approximations for mesoscale continuum mechanical fluxes (such as stress) in terms of primary mesoscopic variables (such as average density and velocity). Our closure construction is based on iterative regularization methods for solving first kind integral equations. Such integral equations are relevant because the mesoscopic density and velocity are related to the corresponding microscopic quantities via a linear convolution operator. The problem of inverting convolution operators is unstable (ill-posed) and requires regularization. Use of the well known Landweber iterative regularization yields successive approximations, of orders zero, one, two and so forth, to the interpolants of particle positions and velocities in terms of the available averages. Closure is achieved by inserting any of these approximations into the equations for fluxes instead of the actual particle positions and velocities. Low order

approximations are simpler to implement, while higher order approximations can be used to more accurately reproduce the high frequency content of the microscopic quantities.

The above general strategy is applied in this paper to spatially averaged dynamics of classical particle chains. We focus on the simplest zero-order approximation and show numerically that it works reasonably well as long as the initial conditions have small velocity fluctuations. The case of large fluctuations in velocities should be handled by higher order approximations.

Acknowledgements

The work of Alexander Panchenko was supported in part by DOE grant DE-FG02-05ER25709 and by NSF grant OISE-0438765. The work of R.P. Gilbert was supported in part by NSF grants OISE-0438765 and DMS-0920850, and by the Alexander v. Humboldt Senior Scientist Award at the Ruhr Universitat Bochum.

References

[1] A.I. Murdoch, D. Bedeaux, Continuum equations of balance via weighted averages of microscopic quantities, Proc. R. Soc. Lond. A 445 (1994) 157–179.
[2] A.I. Murdoch, D. Bedeaux, A microscopic perspective on the physical foundations of continuum mechanics — part I: macroscopic states, reproducibility, and macroscopic statistics, at prescribed scales of length and time, Internat. J. Engrg. Sci. 34 (10) (1996) 1111–1129.
[3] A.I. Murdoch, D. Bedeaux, A microscopic perspective on the physical foundations of continuum mechanics II: a projection operator approach to the separation of reversible and irreversible contributions to macroscopic behaviour, Int. J. Eng. Sci. 35 (10/11) (1997) 921–949.
[4] A.I. Murdoch, A critique of atomistic definitions of the stress tensor, J. Elasticity 88 (2007) 113–140.
[5] J.H. Irving, J.G. Kirkwood, The statistical theory of transport processes IV. The equations of hydrodynamics, J. Chem. Phys. 18 (1950) 817–829.
[6] W. Noll, Der Herleitung der Grundgleichungen der Thermomechanik der Kontinua aus der statistischen Mechanik, J. Ration. Mech. Anal. 4 (1955) 627–646.
[7] R.J. Hardy, Formulas for determining local properties in molecular-dynamics simulations: shock waves, J. Chem. Phys. 76 (1982) 622–628.
[8] H.W. Engl, M. Hanke, A. Neubauer, Regularization of Inverse Problems, Kluwer Academic, Dordrecht, 1996.
[9] C.W. Groetsch, The Theory of Tikhonov Regularization for Fredholm Equation of the First Kind, Pitman, Boston, 1984.
[10] A. Kirsch, An Introduction to the Mathematical Theory of Inverse Problems, Springer, New York, 1996.
[11] V.A. Morozov, Methods for Solving Incorrectly Posed Problems, Springer, New York, 1984.
[12] A.N. Tikhonov, V.Y. Arsenin, Solutions of Ill-Posed Problems, Wiley, New York, 1987.
[13] V. Fridman, A method of successive approximations for Fredholm integral equations of the first kind, Uspekhi Mat. Nauk 11 (1956) 233–234 (in Russian).
[14] L. Landweber, An iteration formula for Fredholm integral equations of the first kind, Amer. J. Math. 73 (1951) 615–624.
[15] G.A. Pavliotis, A.M. Stuart, Multiscale Methods. Averaging and Homogenization, Springer, 2008.
[16] H.W. Engl, On the choice of the regularization parameter for iterated Tikhonov regularization of ill-posed problems, J. Approx. Theory 49 (1987) 55–63.